BIOCHEMISTRY
including biophysical chemistry & molecular biology
Article

Biochemistry **2009,** *48,* 4115–4125 4115
DOI:10.1021/bi9002327

The Mechanism of Domain Alternation in the Acyl-Adenylate Forming Ligase Superfamily Member 4-Chlorobenzoate: Coenzyme A Ligase[†,‡]

Rui Wu,[#] Albert S. Reger,[§,⊥] Xuefeng Lu,[#] Andrew M. Gulick,*[,§,⊥] and Debra Dunaway-Mariano*[,#]

[#]*Department of Chemistry, University of New Mexico, Albuquerque, New Mexico 87131,* [§]*Hauptman-Woodward Medical Research Institute and* [⊥]*Department of Structural Biology, State University of New York, University at Buffalo, Buffalo, New York 14203*

Received February 11, 2009. Revised Manuscript Received March 23, 2009

ABSTRACT: 4-Chlorobenzoate:CoA ligase (CBL) belongs to the adenylate-forming family of enzymes that catalyze a two-step reaction to first activate a carboxylate substrate as an adenylate and then transfer the carboxylate to the pantetheine group of either coenzyme A or an acyl-carrier protein. The active site is located at the interface of a large N-terminal domain and a smaller C-terminal domain. Crystallographic structures have been determined at multiple steps along the reaction pathway and form the basis for a proposal that the C-terminal domain rotates by ~140° between the two states that catalyze the adenylation and thioester-forming half-reactions. The domain rotation is accompanied by a change in the main chain torsional angles of Asp402, a conserved residue located at the interdomain hinge position. We have mutated the Asp402 residue to Pro in order to test the impact of reduced main chain flexibility at the putative hinge position. The crystal structure of the D402P mutant shows that the enzyme adopts the proposed adenylate-forming conformation with very little change to the overall structure. To examine the impact of this mutation on the ability of the enzyme to catalyze the complete reaction, single turnover kinetic experiments were performed. Whereas the ability of this mutant to catalyze the adenylate-forming half-reaction is reduced by ~3-fold, catalysis of the second half-reaction is reduced by 4 orders of magnitude. The impact of the alanine replacement of Asp402 on the thioester-forming reaction is significant, although not as dramatic as the proline mutation, and provides evidence that the Asp402 carboxylate group, through ion pair formation with N-terminal domain residue Arg400, assists in the transition to the thioester-forming conformer. Together these results support the domain alternation hypothesis.

*Address correspondence regarding the reported biochemical studies to D.D.-M. Phone: 505-277-3383; fax: 505-277-6202; e-mail: dd39@unm.edu and correspondence regarding the reported protein structural studies to A.M.G. Phone: (716) 898-8619; fax: (716) 898-8660; e-mail: gulick@hwi.buffalo.edu.

[†]This work was supported by NIH Grant GM-028688 to D.D.M. and by NIH Grant GM-O68440 to A.M.G. The protein structure determination was conducted at the Cornell High Energy Synchrotron Source (CHESS) which is supported by the National Science Foundation under award DMR 0225180 and the National Institutes of Health through its National Center for Research Resources under award 5 P41 RR001646-23.

[‡]The structure factors and coordinates of the CBL D402P mutant bound to 4-chlorobenzoate have been deposited in the Protein Data Bank (Accession code 3DLP).

[1]Abbreviations: CBL, 4-chlorobenzoate:CoA ligase; 4-CB, 4-chlorobenzoate; CoA, coenzyme A; 4-CB-AMP, 4-chlorobenzoyl-adenosine-5′-monophosphate; 4-CB-CoA, 4-chlorobenzoyl-coenzyme A; 4-CP-CoA, 4-chlorophenacyl-coenzyme A; PP_i, inorganic pyrophosphate; ATP, adenosine-5′-triphosphate; AMP, adenosine-5′-monophosphate; PheA, the phenylalanine activating domain of gramicidin synthetase A from *Bacillus brevis*; Acs, acetyl-CoA synthetase from *Salmonella enterica*; IPTG, isopropyl β-D-1-thiogalactopyranoside; RPM, revolutions per minute; rms, root-mean-square; NADH, β-nicotinamide adenine dinucleotide; PEP, phosphoenol pyruvate; DTT, dithiothreitol; K^+ HEPES, potassium salt of *N*-(2-hydroxyethyl)piperzine-*N*′-2-ethanesulfonate; SDS−PAGE, sodium dodecylsulfate−polyacrylamide gel electrophoresis.

4-Chlorobenzoate:CoA ligase (CBL, EC 6.2.1.33)[1] catalyzes the conversion of 4-chlorobenzoate (4-CB) to 4-chlorobenzoyl-coenzyme A (4-CB-CoA) with a consumption of one molecule of ATP. This reaction constitutes the first step of the three-step hydrolytic dehalogenation pathway of 4-CBA leading to the metabolite 4-hydroxybenzoate (*1*−*3*). Previous studies have shown that CBL catalysis occurs via two partial reactions (Scheme 1) (*2*, *4*). The first partial reaction is adenylation of 4-CB by ATP to form the 4-CB-AMP mixed anhydride intermediate, and the second partial reaction is the acyl transfer from the mixed anhydride to the CoA thiol to form the 4-CB-CoA product. The X-ray structure determination of the CBL from *Alcaligenes* sp. AL3007 complexed with 4-CB (*5*) showed that this enzyme is a member of a large family of ligases known as the AMP-binding enzyme superfamily (PF00501). The family fold consists of two α,β-domains: a large N-terminal core domain (CBL residues 1−400) and a smaller C-terminal cap domain (CBL residues 403−504) (*6*, *7*).

The CBL active site is located at the domain−domain interface. 4-CB and ATP bind entirely within the N-terminal domain. The CoA nucleotide binds at the

Published on Web 3/25/2009

Scheme 1

Adenylation Partial Reaction

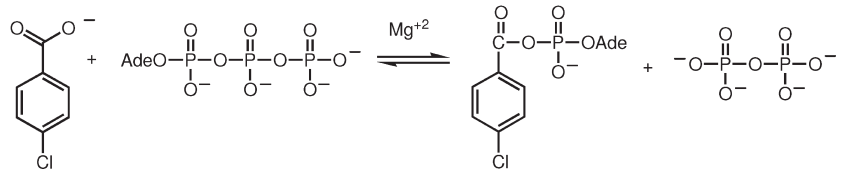

Thioesterification Partial Reaction

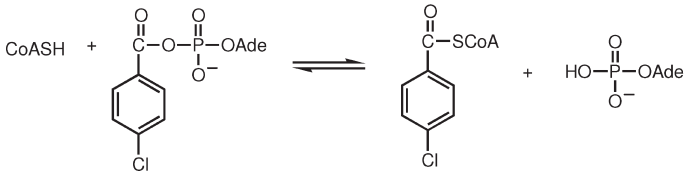

surface of the C-terminal domain, whereas the pantetheine arm passes through a tunnel formed by residues from both domains, which leads to the adenylate binding site of the N-terminal domain (Figure 1).

The structures of the CBL complexed with 4-CB (*5*) or with the adenylate intermediate 4-CB-AMP (*4*) reveal the enzyme in a conformation hereafter referred to as conformation 1 (Figure 1A). A second conformation, conformation 2, has been observed for CBL bound to the product analog 4-chlorophenacyl-CoA and AMP (*8*) (Figure 1B). These alternate conformations have been observed for other members of the enzyme superfamily (*6*, *7*, *9*−*14*). The relative orientations of the two domains in conformations 1 and 2 differ by a ~140°, and consequently the region or "face" of the C-terminal cap domain which interfaces with the N-terminal core domain to complete the active site is different in the two conformations. Kinetic analysis of luciferase (*15*) and acetyl-CoA synthase (Acs) (*16*) site-directed mutants provided the first independent evidence that alternation of the cap domain occurs during the catalytic cycle. Recently, we employed transient kinetic methods to determine the rate constants governing the two partial reactions catalyzed by CBL and CBL cap domain site directed mutants (*4*). In this manner we were able to correlate catalysis of the adenylation partial reaction with cap domain residues that specifically contribute to the active site in conformation 1, and catalysis of the thioesterification partial with cap domain residues that specifically contribute to the active site in conformation 2.

The work described in this paper was carried out for the purpose of determining the mechanics of the CBL C-terminal domain alternation that takes place as the enzyme switches between conformation 1 and conformation 2. The C-terminal domain initiates with a two-stranded antiparallel sheet (shown in yellow in Figure 1) formed by Met404-Ser407 and Glu410-His413. These two strands are an integral part of the C-terminal domain, which rotates as a rigid body; the rms displacement of all Cα positions of the two C-terminal domains is 0.6 Å (Figure 1C). The N-terminal domain terminates with a distorted β-sheet (Figure 1); the final strand of this sheet is formed by residues Val395-Arg400. The peptide segment

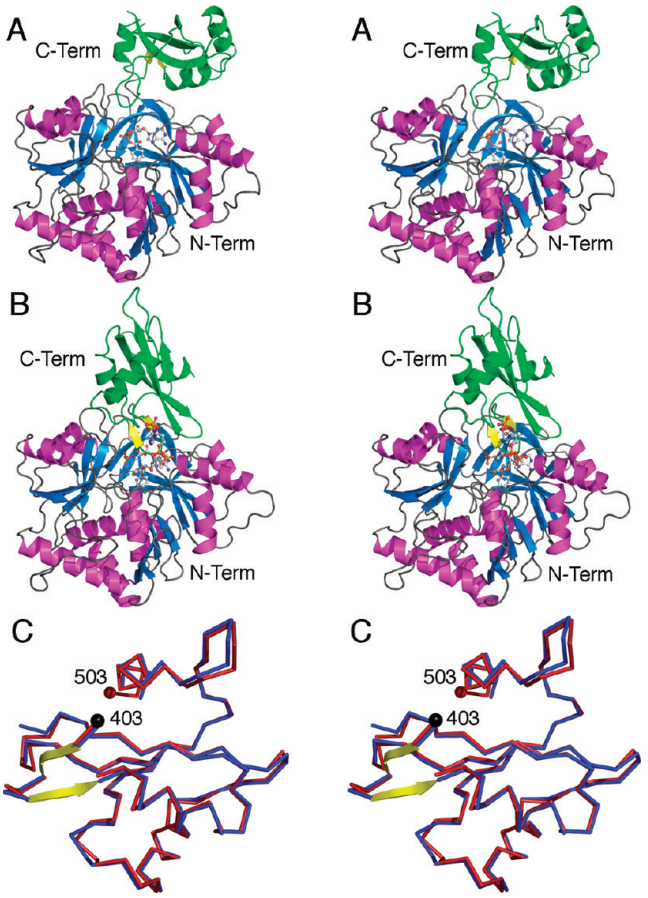

FIGURE 1: (A) Stereorepresentation of the ribbon diagram of CBL complexed with 4-CB-AMP (3CW8) generated from the coordinates of the X-ray structure (*8*). This structure represents conformation 1. (B) A ribbon diagram of the CBL enzyme complexed with 4-chlorophenacyl-CoA (4-CP-CoA) and AMP (3CW8) in conformation 2 (*8*). In both panels, the larger N-terminal domain is shown with blue sheets and magenta helices; the C-terminal domain is shown in green. The antiparallel, two-stranded turn that follows the hinge residue is shown in yellow. Active site ligands are shown in ball-and-stick representation. (C). Stereorepresentation of the alignment of the C-terminal domains derived from the two conformations. Shown in blue is the C-terminal domain of conformation 1, while the domain from conformation 2 is shown in red. The black sphere represents the Cα position of Asp403, and the red sphere represents the C-terminus at Ser503. Shown in yellow are the two sheets that form the antiparallel turn at the start of the C-terminal domain.

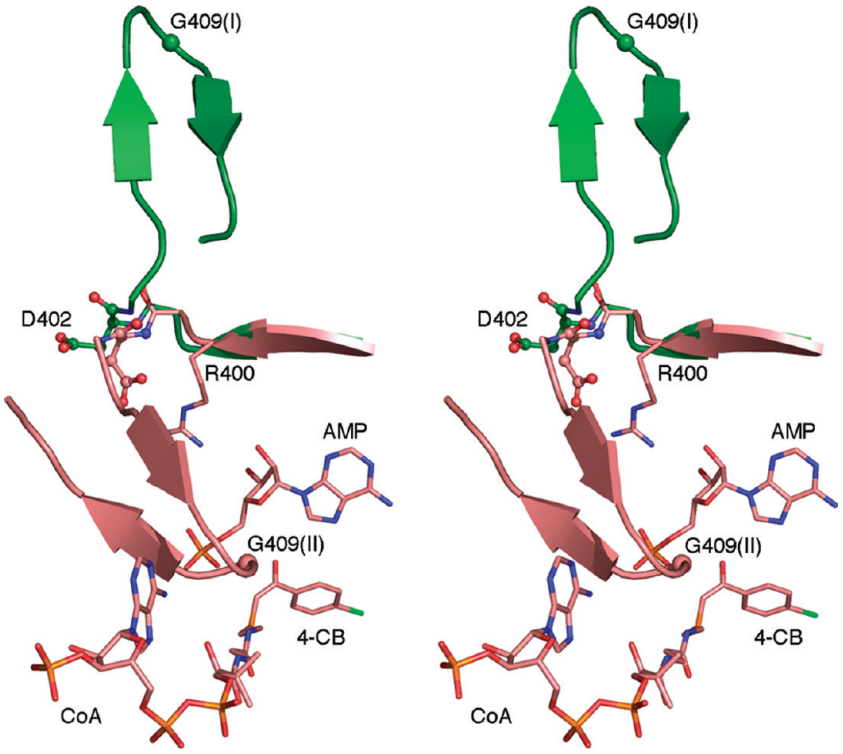

FIGURE 2: Stereorepresentation of the conformational change that occurs in CBL, comparing 3CW8 (conformation I) to 3CW9 (conformation 2). The structures were superimposed based on the N-terminal domain. Protein residues 397−414 are shown as cartoon representation. This region encompasses the final strand of the N-terminal domain at Val395-Arg400, the hinge region at Asp402, and the antiparallel turn containing β-strands at Ile405-Ser407 and Glu410-Ile412. The adenylate-forming conformation 1 is shown in green, while the thioester-forming conformation 2 is shown in pink. The AMP and 4-chlorophenacyl-CoA ligands that are present in conformation 2 are shown in stick representation, as is the side chain of Arg400 from conformation 2. Asp402, the hinge residue, is shown in ball-and-stick representation for both conformations. The Cα position of Gly409, a universally conserved residue on the turn that joins the two strands, is shown with a sphere.

that connects the two domains is three residues long (401−403), too short to be called a "linker", and instead we will refer to the region as the "hinge". The main chain dihedral angles of the residues of the hinge demonstrate that the residue that undergoes the most significant conformational change is Asp402 (Figure 2). In the adenylate-forming conformation, the residues from 401 to 403 form a type III β-turn. In this conformation, a hydrogen bond is formed between the carbonyl of Arg400 and the main chain amide of Asp403. In the conformation that is used for the thioester-forming half-reaction, the ϕ angle of Asp402 shows a small rotation, changing from −66° to −89°. Accompanying this change in ϕ is a larger rotation of the Asp402 ψ angle from −29° to −164°, which accounts for the majority of the domain rotation observed in the two conformational states. The rotation to the new ψ angle breaks the backbone amide hydrogen bond of the type III turn observed in conformer 1, forming in its place an ion pair between the side chains of Asp402 and Arg400 that stabilizes conformer 2.

In this study we focused our attention on the role of the interdomain hinge in CBL catalysis. The Asp402 hinge residue accounts for the majority of the conformational change associated with domain alternation, and therefore we investigated the effect of replacing this residue with proline, which has a restricted ϕ angle near −70° (*17*). We hypothesized that if residue 402 is the true hinge, the restriction of the ϕ angle in the D402P mutant will prevent efficient domain alternation. In order to test this hypothesis, we measured the rate constants governing the respective partial reactions in the D402P mutant. We also explored the importance of Asp402-Arg400 ion pair in facilitating the thioester-forming partial reaction through stabilization of conformer 2 via kinetic analysis of the D402A mutant. Herein, we report first on the structure and kinetic properties of the D402P CBL mutant, and second, on the kinetic properties of the D402A mutant. We interpret our results as evidence that the flexibility at the 402 main chain position is critical for the transition from the adenylate-forming conformer to the thioester-forming conformer, and that the Asp402-Arg400 ion pair formation is required for efficient catalysis of the thioester-forming partial reaction.

MATERIALS AND METHODS

Wild-Type and CBL Protein Preparation. The His-tagged wild-type CBL from *Alcaligenes sp. AL3007* was prepared as described in ref *5*. The ligase mutant cDNAs were prepared using the *Sph*I-*Bgl*II-pQE-70-CBL clone as the template and commercial primers in the PCR reaction. The purified PCR product was digested with *Sph*I and *Bgl*II (Invitrogen, Carlsbad CA) and ligated to *Sph*I and *Bgl*II digested *Sph*I-*Bgl*II-pQE-70-CBL. The gene sequence was verified by DNA sequencing at the Center for Genetics in Medicine, University of New Mexico School of Medicine, Albuquerque, NM.

A single colony of *Escherichia coli* JM109 containing the plasmid *Sph*I-*Bgl*II-pQE-70-D402P CBL was used to inoculate 10 mL of LB medium containing 50 μg/mL ampicillin at 37 °C and 250 RPM. The 10 mL culture was

then used to inoculate 10 L of fresh LB medium containing 50 μg/mL ampicillin, and the culture was grown at 20 °C and 200 RPM. After 26 h (O.D. ~0.7 at 600 nm) IPTG was added to a final concentration of 1 mM. Following 10 h the cells were harvested by centrifugation at 5000*g* for 15 min. The 10 g of wet cells were suspended in 100 mL of lysis buffer (50 mM NaH_2PO_4, pH 8.0, 10 mM imidazole, 1 mM DTT) containing 10 μL of 0.1 mM the protease inhibitor PMSF. The cell suspension was passed through a French press at 1200 pounds per square inch and then centrifuged at 48000*g* and 4 °C for 30 min. The supernatant was loaded onto a Ni-NTA Agarose column (QIAGEN, 25 mL) that had been pre-equilibrated with the lysis buffer. The column was eluted with 500 mL of wash buffer (50 mM NaH_2PO_4, pH 8.0, 50 mM imidazole, 1 mM DTT) and then eluted with 200 mL of elution buffer (50 mM NaH_2PO_4, pH 8.0, 250 mM imidazole, 1 mM DTT). The protein was dialyzed for 3 h against three changes of 1.5 L of 50 mM K^+HEPES (pH = 7.5) containing 1 mM DTT. The protein purity was verified by SDS−PAGE analysis. The protein concentration was calculated from the protein absorbance at 280 nm using the extinction coefficient = 27760 M^{-1} cm^{-1}. The yields of CBL D402P and D402A mutants were 1 and 6 mg/g of wet cell, respectively.

Crystallization of D402P CBL. Protein at 10 mg/mL was combined with ATP and 4-CB to a final concentration of 1 mM each. Crystals were grown by hanging-drop vapor diffusion at 4 °C using a precipitant containing 16−24% pentaerythritol propoxylate 426 (*18*), and 0.1 M K^+HEPES (pH 6.5 or 6.75) and an equal volume of protein and precipitant in the drops. Crystals were cryoprotected by transferring through six solutions containing protein ligands and increasing amounts of ethylene glycol for approximately 1 min each. The final cryoprotectant contained 24% pentaerythritol propoxylate 426, 24% ethylene glycol, and 0.1 M K^+HEPES and 1 mM each of ATP and 4-CB.

Crystallographic Data Collection and Structure Refinement. Data for D402P CBL were collected at the Cornell High Energy Synchrotron Source at Cornell University at beamline F2. The data were processed with MOSFLM (*19*) to 2.6 Å. The Wilson B-value was 76 $Å^2$; the data exhibited anisotropic behavior with diffraction weaker parallel to the 3-fold axis. The structure was solved by molecular replacement using MOLREP (*20*) of the CCP4 package (*21*) using the prior CBL structure (1T5H) as a search model with all nonprotein atoms removed. Refinement was performed with REFMAC5 (*22*). The density at the active site showed clear density for the 4-CB molecule. Although we had incubated the enzyme with both ATP and 4-CB, there was very weak density for the nucleotide portion of the ligand. This is similar to the original structure of CBL in which 4-CB and AMP were included in the crystallization cocktail and only 4-CB was modeled (*5*).

Isotropic B-factor analysis was used to justify inclusion of the 4-CB molecule. The average B-factor for 4-CB ligand was 58 $Å^2$, while the average B-factor for all protein atoms was 59 $Å^2$. The B-value of the protein atoms that form the aryl binding pocket is 40 $Å^2$. Attempts to include AMP in the model resulted in B-factors that were 20−30 $Å^2$ greater than the 4-CB ligand and unsatisfactory $2F_o - F_c$ density. Additionally, a stretch of residues that borders the adenine binding pocket, Ala280-Ala282, adopts the conformation seen in the unliganded or 4-CB binary complex and not the conformation observed in the nucleotide bound states (*8*). AMP was therefore not included in the final model, although it may be present at partial occupancy. TLS anisotropic refinement was included late in the final refinement, with the N- and C-terminal domains defined as independent groups (*23*), and was monitored by a drop in the R-free value.

Steady-State Kinetics. The 4-CB-CoA ligase activity was measured at 25 °C by using a direct continuous spectrophotometric assay (*24*) wherein the increase in the absorbance of the 1 mL reaction solution resulting from the conversion of 4-CB to 4-CB-CoA was monitored at 300 nm ($\Delta\epsilon$ = 4.1 $mM^{-1}cm^{-1}$). The 1 mL assay solution contained wild-type or mutant CBL and saturating concentrations of 4-CB (2 mM), CoA (1 mM), ATP (3.5 mM), $MgCl_2$ (15 mM) in 50 mM K^+HEPES (pH 7.5) at 25 °C. For V_{max} and K_M determinations the initial velocity was measured as a function of one substrate concentration (varied from 0.5- to 5-fold K_M) at fixed saturating concentrations of the cosubstrates. The k_{cat} was calculated from the ratio of V_{max} and enzyme concentration.

$$V = V_{max}[S]/([S] + K_M) \quad (1)$$

where V is the initial velocity, V_{max} the maximum velocity, [S] the substrate concentration, K_M the Michaelis constant.

Transient-State Kinetics. Single turnover reactions were carried out at 25 °C using a KinTek rapid quench instrument to mix 13 μL of 60 μM wild-type or mutant CBL in 50 mM K^+HEPES (pH 7.5) with 14 μL of 16 μM [carboxyl-^{14}C]4-CB (specific activity = 50−60 mCi/mmol) (American Radiolabeled Chemicals, Inc.), ATP (7 mM), $MgCl_2$ (30 mM), and CoA (2 mM for wild-type and D402P CBL and 30 mM for D402A CBL) in 50 mM K^+HEPES (pH 7.5). Reactions were terminated using 193 μL of 0.1 N HCl as the quench. The reactants and products were separated by HPLC and quantitated by liquid scintillation counting as described previously (*4*). The rate data measured for a single turnover reaction of [carboxyl-^{14}C]4-CB and ATP were fitted with the first-order eqs 2 and 3 using the Kaleidagraph program (Synergy Software, Reading, PA).

$$[S]_t = [S]_{max} - ([P]_{max}(1 - e^{-kt})) \quad (2)$$

$$[P]_t = [P]_{max}(1 - e^{-kt}) \quad (3)$$

where k is the first-order rate constant; $[S]_t$ and $[P]_t$ are the substrate and product concentrations at time "t", respectively. The rate data measured for the single-turnover reaction of [carboxyl-^{14}C]4-CB, ATP, and CoA were fitted to a simplified kinetic model (see Scheme 2) by using the simulation program KINSIM (*25*).

The time course for the multiple turnover reaction catalyzed by wild-type or D402P CBL was measured for a reaction solution initially containing 10 μM enzyme,

Scheme 2

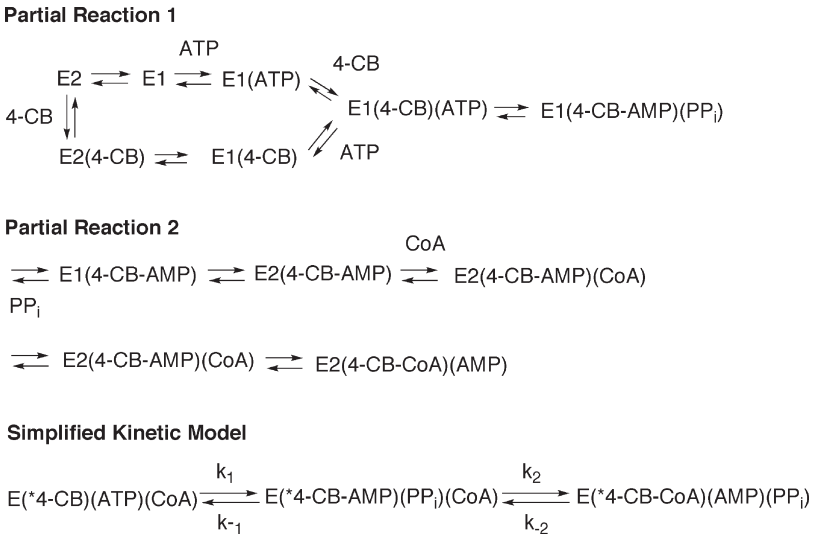

40 μM [^{14}C]4-CB, 500 μM ATP, 500 μM CoA, and 12 mM $MgCl_2$ in 50 mM K^+ HEPES (pH 7.5). The data measured for the D402P CBL were fitted to eqs 2 and 3, whereas the data measured for the wild-type CBL were fitted to eq 4 using the program Kaleidagraph.

$$P_t = P_0 - E[A_0(1 - \exp(-(k_1 + k_2)t) + (k_1k_2/(k_1 + k_2))t] \quad (4)$$

where P_t and P_0 are the concentration of the product at time t and zero, E is the final concentration of enzyme active sites, k_1 and k_2 are rate constants of the fast and slow reaction steps in the reaction pathway; A_0 is equal to k_1 divided by the sum of k_1 and k_2.

RESULTS AND DISCUSSION

Structure Determination of the D402P CBL. The D402P mutant enzyme crystallized in the isomorphic space group observed previously with the *apo* wild-type CBL and its complex with 4-CB or 4-CB-AMP that define conformation 1. The structure was determined by molecular replacement and refined against the observed data. The final model contains residues 1−502 and a single 4-CB ligand. The 21 waters included in the final D402P model had well-defined density and hydrogen-bonding partners. The final refinement statistics are presented in Table 1. Electron density maps of the linker mutation site and the active site are shown in Figure 3A and 3B, respectively.

The D402P CBL model shows the same two-domain structure reported for wild-type CBL. The rms distance between the corresponding Cα positions in the D402P CBL(4-CB) complex and the wild-type CBL(4-CB-AMP) complex is 0.6 Å over the full length of the protein (Figure 4). The orientation of the C-terminal domain relative to the N-terminal domain is similar to that observed in the wild-type CBL *apo*, 4-CB-bound, and 4-CB-AMP-bound forms that define conformation 1. Indeed, the ϕ/ψ angles of the residues that form and immediately surround the hinge region are quite similar in the wild-type CBL(4-CB-AMP) complex and in the D402P CBL(4-CB) complex (Table 2). This includes the mutation site residue 402: for the wild-type Asp402, the ϕ/ψ angles are −66 and −32, while for the mutant Pro402 the torsion angles are −62 and −26. The ϕ/ψ angles of both aspartate and proline at position 402 fall within a favored region of the Ramachandran plot for the respective amino acid (*17*).

Table 1: Crystallographic and Refinement Statistics for the D402P CBL (4-CB) Complex

	D402P + 4-CB
resolution	30−2.6 Å
space group	$P3_221$
unit cell	a = 128.0 Å
	b = 128.0 Å
	c = 71.2 Å
R_{merge}[a]	7.2% (47.9%)
completeness[a]	94.8% (96.1%)
I/σ[a]	22.4 (2.6)
# observations	173679
# reflections	19751
R_{cryst} (overall/highest resolution shell)[a]	19.9% (35.5%)
R_{free} (overall/highest resolution shell)[a]	25.7% (37.9%)
rms deviation bond lengths, angles	0.016 Å, 1.64°

[a] Values for the highest resolution shell are given in parentheses.

In an earlier study, we identified the active site residues that contribute most significantly to catalysis of partial reaction 1 in conformer 1 and to catalysis of partial reaction 2 in conformer 2. We show in Figure 4C a superposition of the residues most important to catalysis of partial reaction 1 as defined by the structure of the wild-type CBL(CB-AMP) complex and the D402P CBL (CB) complex. The only difference between the adenylate binding pocket of the two structures is in the loop containing Asp280-Thr283, which in the mutant fills the vacant adenine site. This alternate loop conformation is also observed in the structure of the wild-type CBL(4-CB) complex (*5*) and therefore we believe that it is not related to the mutation. Because the positions of the catalytic residues are conserved in the mutant, it

Table 2: Backbone Torsion Angles (ϕ/ψ) and Secondary Structure for the CBL Hinge Region and Its Flanking Residues, As Observed in the Wild-Type CBL(4-CB-AMP) Structure (Wt Conf1) (3CW8 (*8*)), the Wild-Type CBL(4-CP-CoA)(AMP) Structure (Wt Conf2) (3CW9 (*8*)) and the D402P CBL(4-CB) Structure (3DLP)

residue	secondary structure[a]	Wt Conf1(ϕ,ψ)[a]	Wt Conf2 (ϕ,ψ)[a]	D402P (ϕ,ψ)[a]
Val395	strand	−95, 118	−105, 128	−106, 122
Arg396	strand	−91, 118	−104, 118	−100, 117,
Ile397	strand	−79, 128	−82, 122	−78, 121
Leu398	strand	−103, −37	−106, −28	−96, −39
Gly399	strand	156, 179	157, −166	160, −175
Arg400	strand	−68, 139	−96, 147	−82, 140
Val401	turn	−57, −41	−72, −41	−53, −49
X402[b]	turn	−66, −32	−89, −164	−62, −26
Asp403	turn	−81, −15	−101, 17	−87, −8
Met404	coil	−64, 138	−61, 133	−66, 133
Ile405	strand	−106, 138	−100, 140	−107, 141
Ala406	strand	−113, 103	−121, 110	−125, 115
Ser407	strand	−127, 113	−124, 124	−115, 90
Gly408	turn	49, 57	59, 25	64, 61
Gly409	turn	74, 10	79, 11	95, −41
Glu410	strand	−125, 137	−106, 130	−92, 126
Asn411	strand	−72, 131	−76, 124	−76, 137
Ile412	strand	−133, 125	−130, 124	−134, 129
His413	coil	−102, 116	−90, 137	−111, 107

[a] Torsion angle calculation and secondary structure prediction were performed by STRIDE (*28*). Residues 401−403 are technically classified as a 3_{10} helix for the wild-type structure in conformation 1; however, it can also be classified as a type 3 turn because it encompasses just a single turn of the helix. The (ϕ,ψ) angles are listed as units of degrees. [b] X = Asp in wild-type CBL and Pro in the D402P CBL.

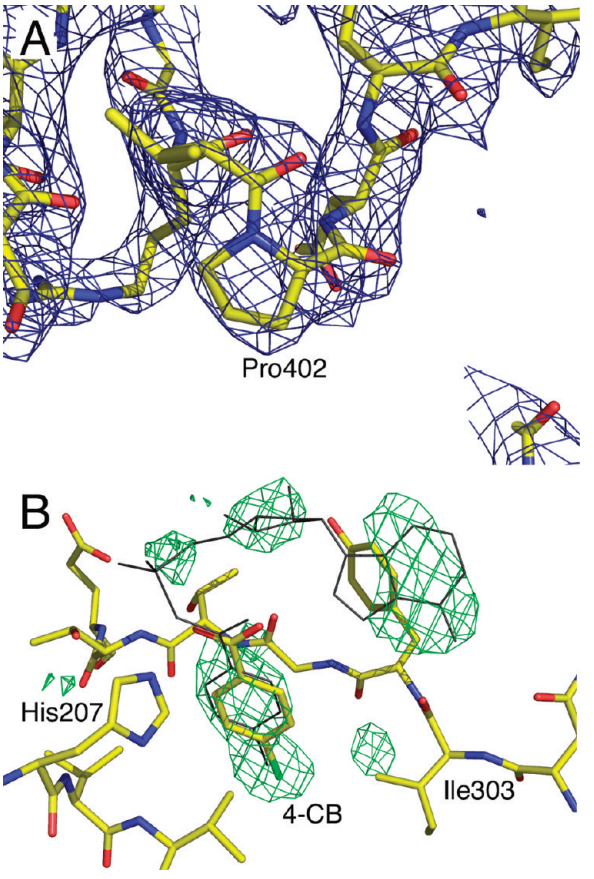

FIGURE 3: Representative electron density. (A) Electron density is shown for the D402P mutation of the final refined model using the $2F_o - F_c$ coefficients and contoured at 1σ. (B) Omit map electron density was calculated with coefficients of the form $F_o - F_c$ after removing the ligand and submitting the model to a cycle of refinement with REFMAC. The map is shown contoured at 3σ.

should display efficient catalysis of the adenylate-forming partial reaction.

The backbone torsion angles (ϕ/ψ) for the CBL hinge region and its flanking residues (Table 2) illustrate the changes that occur when the wild-type CBL rotates from conformation 1 to conformation 2. For the switch in the wild-type CBL, Asp402 rotates from ϕ/ψ angles −66 and −32 in conformation 1 to ϕ/ψ angles −89 and −164 in conformation 2. Rotation of the ψ torsion angle from −32° to −164° in the wild-type CBL is accompanied by contact between the carbonyl oxygen atoms of Asp402 and Val401 (Figure 5). To avoid this steric clash, a rotation about the bond between the Cα and N of Asp 402 must precede (or occur coincident with) the rotation about the bond between Cα and the carbonyl C, as depicted by the movie in Supporting Information. Comparison of the two crystallographic structures of the wild-type CBL suggests that the Asp402 ϕ angle must rotate from −66 to −89 to avoid the clash between the carbonyl groups of residues 401 and 402.

Proline residues have significantly constrained ϕ angles due to the presence of the imine ring of the side chain, the planar trigonal bonding of the imine nitrogen, and the tetrahedral configuration of the Cα bonding (*26*). Proline residues in well-determined, high resolution crystal structures are observed in one of two puckered configurations, UP and DOWN. These configurations are energetically favored, allowing the bond angles to approach the tetrahedral bonding angle of 109.5° (*27*). Significant energetic barriers exist in minor torsional rotations around the bonds within the proline ring that disrupt these most favored puckered configurations. These geometric constraints result in a ϕ angle for proline residues that is ∼60° and limit even minor rotations to the backbone torsion angles (*27*). The impact of this

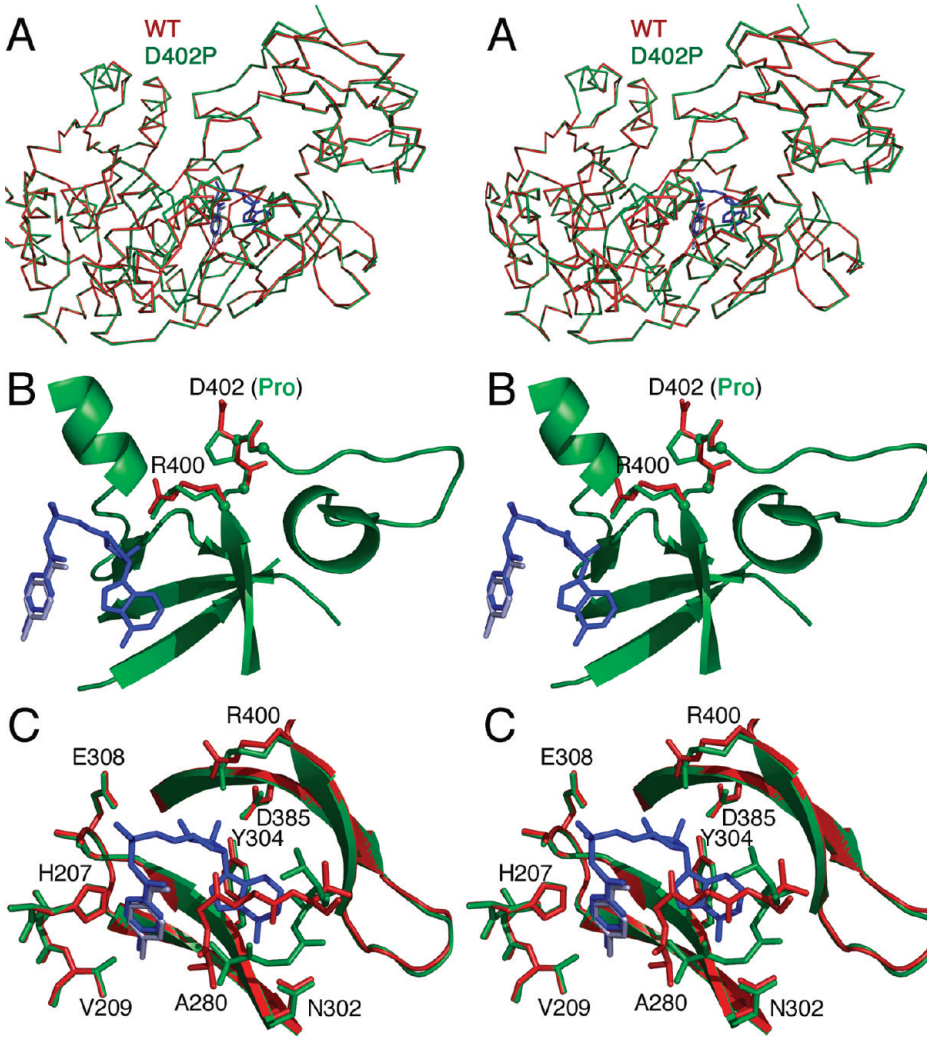

FIGURE 4: Structure comparison of the wild-type and D402P CBL proteins. (A) A stereorepresentation of the Cα trace of the wild-type protein (red) and D402 mutant protein (green). Shown in dark blue is the 4-CB-AMP ligand of the wild-type structure, while shown in light blue is the 4-CB molecule from the mutant. (B) Stereorepresentation of the hinge region of the mutant (green) protein. Several secondary structural elements are shown from the mutant enzyme. Superimposed on the hinge residues is the hinge from the wild-type enzyme in the adenylate-forming conformation. The green spheres represent the Cα positions of Arg400-Val401-Asp402-Asp403 from the mutant structure. The side chains of both Arg400 and the Asp or Pro402 residue are shown. Also included are the ligands from the wild-type (dark blue) or the mutant (light blue) structure. (C) Superposition of the adenylate-binding pocket of wild-type enzyme (red) and the D402P mutant (green). Ligands are colored as in panel B. The loop from Ala280-Thr283 is the only significant difference between the active sites of the two enzymes.

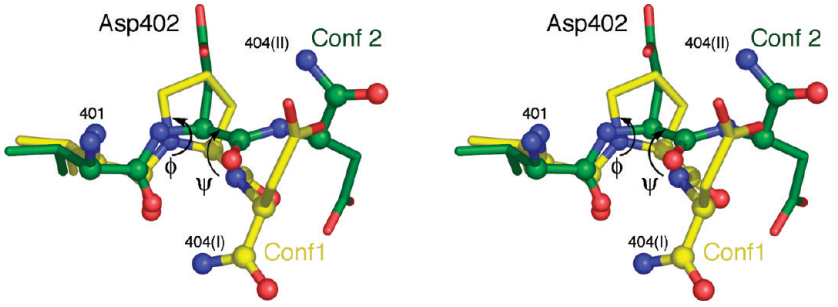

FIGURE 5: Rotations in the main chain torsion angles at the hinge residue that are necessary for the rotation of the C-terminal domain. Superimposed on the structure of the D402P mutant (yellow) is the structure of the wild-type enzyme in conformation 2 (green). The hinge region is shown starting with the amide nitrogen of Val401 and continuing through the amide nitrogen of Met404 (labeled 404(I) or 404(II)). The atoms are colored blue for nitrogen atoms, red for oxygen atoms, and yellow for the carbon atoms of the D402P mutant and green for the carbon atoms of the conformation 2 model. The rotational backbone angles (ϕ and ψ) at residue 402 are indicated. Main chain atoms are shown with spheres, while the side chains are represented as sticks. See also the movie in Supporting Information.

restriction is also shown in the movie in Supporting Information.

The ϕ/ψ angles of the hinge residue in conformation 1 are a commonly observed conformation for proline residues in well-determined, high resolution structures. In contrast, the ϕ/ψ angles of conformation 2 (−89 and −164) fall at the edge of a generously allowed region of the Ramachandran plot for Pro (*17*).

Table 3: The Steady-State Kinetic Constants k_{cat} and K_m Measured for Wild-Type CBL (*4*), D402P CBL and D402A CBL in 50 mM K^+HEPES (pH 7.5, 25 °C) containing 15 mM $MgCl_2$

CBL	substrate	k_{cat} (s^{-1})	K_M (μM)	k_{cat}/K_M (s^{-1} M^{-1})	x-fold decrease in k_{cat}/K_M
wild type	4-CB[a]	9.2 ± 0.2	0.9 ± 0.1	1×10^7	
	CoA[b]	9.3 ± 0.3	310 ± 30	3×10^4	
	ATP[c]	11.5 ± 0.1	124 ± 4	9×10^4	
D402P	4-CB[a]	3.4 (±0.1) × 10^{-2}	1.2 ± 0.1	3×10^4	300
	CoA[b]	3.7 (±0.1) × 10^{-2}	2000 ± 100	2×10^1	1500
	ATP[c]	2.82 (±0.03) × 10^{-2}	13.1 ± 0.7	2×10^3	45
D402A	4-CB[a]	0.96 ± 0.03	2.3 ± 0.2	4×10^5	25
	CoA[b]	1.8 ± 0.2	6000 ± 1000	3×10^2	100
	ATP[c]	1.01 ± 0.01	28.1 ± 0.9	4×10^4	2

[a] For wild-type CBL reaction solutions contained 0.5−10 μM 4-CB, 3.5 mM ATP and 1 mM CoA. For D402 CBL mutants reaction solutions contained 0.8−10 μM 4-CB, 1.5 mM ATP and 10 mM CoA. [b] For wild-type CBL reaction solutions contained 100−1500 μM CoA, 3.5 mM ATP and 2 mM 4-CB. For D402 CBL mutants reaction solutions contained 1.2−5.0 mM CoA, 1.5 mM ATP and 20 μM 4-CB. [c] For wild-type CBL reaction solutions contained 100−800 μM ATP, 2 mM 4-CB and 1 mM CoA. For D402 CBL mutants reaction solutions contained 10−500 μM ATP, 20 μM 4-CB and 10 mM CoA.

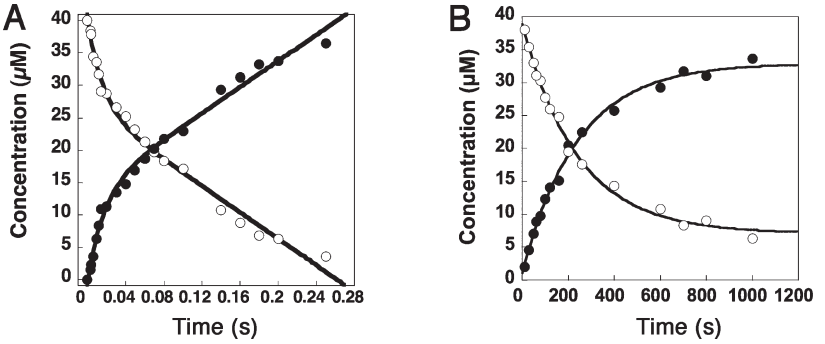

FIGURE 6: Pre-steady-state time course for the wild-type and D402P CBL catalyzed reaction of 4-CB, ATP and CoA depicted as a plot of 4-CB (○) or 4-CB-CoA (●) concentration vs reaction time. The initial reaction solution consisted of 10 μM wild-type CBL, 40 μM [^{14}C]4-CB, 500 μM ATP, 500 μM CoA and 12 mM $MgCl_2$ in 50 mM K^+HEPES (pH 7.5). (A) Wild-type CBL. The data were fitted to eq 4 giving the k_1 for the burst phase 60 ± 10 s^{-1} and for the following turnovers k_2 = 10.2 ± 0.7 s^{-1}. (B) D402P CBL. Data were fitted to a single exponential equation to define an apparent rate constant k = 0.004 ± 0.0003 s^{-1}.

More importantly, the transition between these two states passes through a disallowed region of the proline-specific Ramachandran plot. This suggests that while D402P CBL can exist in both conformational states, the state observed in the adenylate-forming conformation is likely to be much more stable. Additionally, the kinetic energy barrier to the conversion of D402P CBL from conformation 1 to 2 is predicted to be significantly higher than that encountered by the wild-type enzyme. In order to determine the impact of restricting main chain motion at the proposed hinge residue Asp402, we measured the steady-state and transient-state kinetic properties of the D402P CBL mutant.

Kinetic Properties of D402P CBL. The k_{cat} and K_M values of the wild-type CBL and D402P CBL were determined at pH 7.5 and 25 °C by carrying out initial velocity experiments in which the Mg^{2+} activator and two of the substrates were held at a fixed, saturating concentration while the concentration of the third substrate was varied (Table 3). The k_{cat} value is reduced 300-fold in the D402P mutant. For wild-type CBL, release of product from the second partial reaction is 6-fold slower than is the rate of product formation (*4*). In contrast, product release is not rate limiting in the case of D402P CBL (Figure 6), and therefore it appears that the mutation causes a significant reduction in the efficiency of product formation. The CoA k_{cat}/K_M shows by far the largest decrease in value (1500-fold, Table 3), and this indicates that the second partial reaction is inhibited to the greatest extent by the mutation.

In order to measure the reduction in the rates of the individual partial reactions catalyzed by the D402P mutant, single turnover time courses were measured using rapid quench techniques. Wild-type and D402P CBL were reacted with [^{14}C]4-CB and ATP in the presence and in the absence of CoA for specified time periods, following which the reactions were terminated with HCl and the radiolabeled species separated and quantitated. The time courses measured for the single turnover reaction of [^{14}C]4-CB and ATP carried out in the absence of CoA are shown in Figure 7A,B. The data were fitted using first-order rate equations to define the k_{obs} values reported in Table 4. The experimental rate constant k_{obs} is the culmination of the microscopic rate constants governing the substrate binding and chemical steps represented in Scheme 2 for partial reaction 1. The value of k_{obs} is reduced ~3-fold in the D402P mutant.

The time courses for the single turnover reactions carried out in the presence of 1 mM CoA are shown in Figure 8A−C. The time course data for [^{14}C]4-CB consumption were initially fitted with a first-order rate equation to define the k_{obs} values for comparison to those measured for [^{14}C]4-CB consumption in the reactions carried out in the absence of CoA (Table 4). The k_{obs}

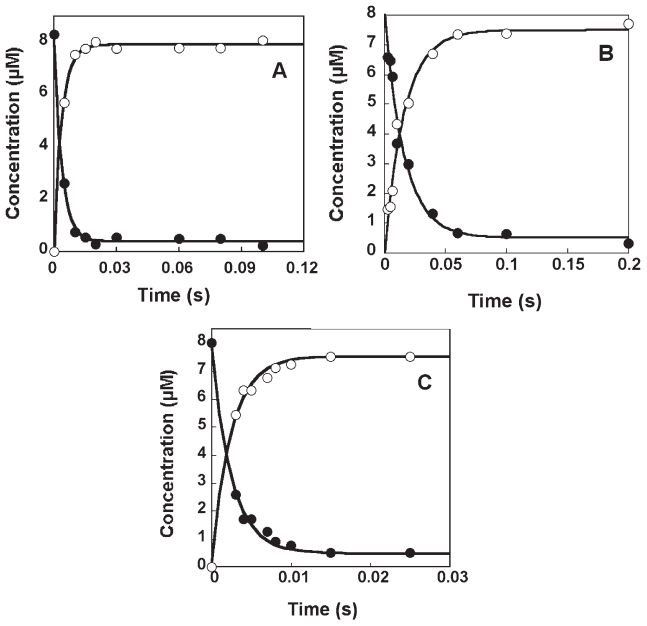

FIGURE 7: Time course for a single turnover reaction of 4-CB and ATP catalyzed by wild-type and mutant CBL in 50 mM K^+ HEPES (pH 7.5, 25 °C). The final concentration of the reactants in the 27 μL reaction mixture are 8.3 μM 4-CBA, 3.6 mM ATP, and 15.6 mM $MgCl_2$ and 29 μM (A) wild type CBL, (B) D402P CBL, (C) D402A CBL. 4-CB (●); 4-CB-AMP (○).

Table 4: The apparent First-Order Rate Constants (k_{obs}) Determined for the 4-CB Consumption Inreactionsolutions Initially Containing 8.3 μM [^{14}C]4-CB, 29 μM Wild-Type or Mutant CBL, 3.6 mM ATP, 15.6 mM $MgCl_2$, and 50 mM K^+HEPES (pH 7.5, 25 °C) in the Absence and in the Presence of CoA[a]

	k_{obs} (s^{-1})[b]	k_{obs} (s^{-1})[c]	k_1 (s^{-1})	k_{-1} (s^{-1})	k_2 (s^{-1})	k_{-2} (s^{-1})
wild-type CBL	270 ± 10	350 ± 40	300	0.01	120	0.1
D402P CBL	84 ± 9	120 ± 20	120	10	0.012	0.002
D402A CBL	400 ± 30	182 ± 8	190	11.2	0.85	0.005

[a] Also listed are the rate constants (k_1, k_{-1}, k_2, k_{-2}), defined in Scheme 2, and derived from single turnover time course data for the reaction solutions initially containing 8.3 μM [^{14}C]4-CB, 29 μM wild-type or mutant CBL, 3.6 mM ATP, 15.6 mM $MgCl_2$, 50 mM K^+HEPES (pH 7.5, 25 °C) and 1 mM or 15 mM CoA. See Materials and Methods for details. [b] Reaction solutions did not contain CoA. [c] Reaction solutions contained 1 mM CoA (wild-type and D402P CBL) or 15 mM CoA (D402A CBL).

values measured in the presence and absence of CoA are not significantly different.

The substrate binding, product dissociation, and chemical steps that, together with the conformational changes, comprise the full single turnover reaction are represented in Scheme 2. The simplified kinetic model used in fitting the time course data by curve simulation with KINSIM (*25*) combines these numerous steps into two steps defining partial reactions 1 and 2 (Scheme 2). We use the rate constants k_1 and k_2 derived from the data fitting to compare the efficiencies of the respective partial reactions. Thus, the replacement of Asp402 with Pro decreases the efficiency of the first partial reaction ~3-fold, and the second partial reaction ~10000-fold.

We conclude that the D402P mutant retains the ability to form the 4-CB-AMP intermediate but not the ability to efficiently convert this intermediate to 4-CB-CoA. The

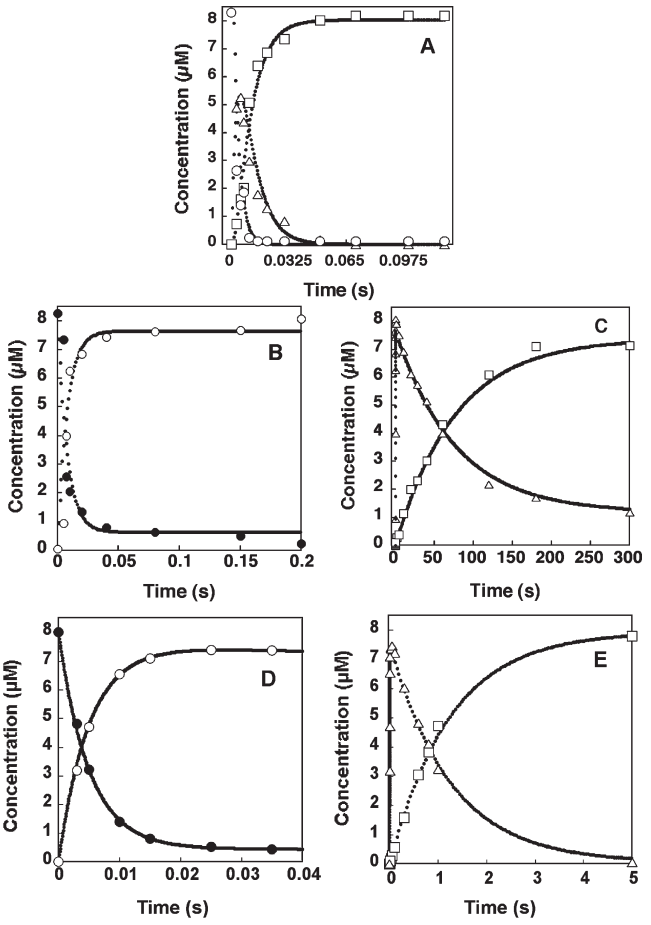

FIGURE 8: Time course for a single turnover of 8.3 μM 4-CB, 3.6 mM ATP, 15.6 mM $MgCl_2$, CoA and 29 μM CBL in 50 mM K^+HEPES (pH 7.5 and 25 °C). (A) Wild-type CBL with 1 mM CoA; 4-CB (○), 4-CB-AMP (Δ), 4-CB-CoA (□). (B, C) D402P CBL with 1 mM CoA; for (B) 4-CB (●), 4-CB-AMP (○); for (C) 4-CB-AMP (Δ), 4-CB-CoA (□). (D, E) D402A CBL with 15 mM CoA: for (D) 4-CB (●), 4-CB-AMP (○); for (E) 4-CB-AMP (Δ), 4-CB-CoA (□). The rate data were fitted to the kinetic model shown in Scheme 2 using KINSIM (*25*).

structure of the D402P CBL is evidence that the mutant forms the same conformation 1 as does the wild-type enzyme. Given that the mutant is able to form 4-CB-CoA, albeit slowly, we can argue that the mutant can also exist in conformation 2. However, we do not know if the mutant CBL conformation 2 is identical to the wild-type CBL conformation 2. Therefore, it is not possible at this time to assign the entire reduction in k_2 to slow switching from conformation 1 to conformation 2. If we are correct in assuming that the conformer interconversion occurs very slowly in D402P CBL, then it follows that the "monophasic" time course measured for the first partial (Figure 7B) indicates that in the absence of ligands, the mutant exists predominantly as conformer 1, as indeed was observed crystallographically (*5*).

Kinetic Properties of D402A CBL. In addition to serving as the key hinge residue Asp402 contributes a carboxylate side chain, which alternates between solvent in conformation 1 and the N-terminal active site residue Arg400 in conformation 2. Arg400 engages in hydrogen bond formation with the 2′-OH of 4-CB-AMP bound to CBL conformer 1. As the Asp402-Arg400 pair are

stringently conserved among CBLs and highly conserved within the superfamily, we wondered if the Asp402 side chain plays a direct role in cap domain alternation by stabilizing conformation 2 though electrostatic interaction with Arg400. To explore this possibility, the Asp402 was replaced with Ala and the kinetic properties of the D402A CBL mutant were determined. First, the D402A mutant is similar to the D402P mutant in that the CoA k_{cat}/K_m shows the largest decrease in value, but compared to the 1500-fold reduction observed for D402P CBL, the 100-fold reduction observed for D402A mutant is less impressive (Table 3). Nonetheless, this result indicates that the second partial reaction is the most effected by the mutation.

The time course measured for the single turnover reaction of [^{14}C]4-CB and ATP carried out in the absence of CoA is shown in Figure 7C and the k_{obs} value derived from the data set is reported in Table 4. A comparison of the k_{obs} values of Table 4 reveals that in contrast to the D402P mutant, which shows a 3-fold decrease in efficiency of catalysis of the first partial reaction, the D402A mutant appears to be slightly more efficient than wild-type CBL. The time courses for the single turnover reactions carried out in the presence of CoA are shown in Figure 8D,E. The time course data for [^{14}C]4-CB consumption were initially fitted with a first-order rate equation to define the k_{obs} values for comparison to those measured for [^{14}C]4-CB consumption in the reactions carried out in the absence of CoA (Table 4). The k_{obs} value measured in the presence of CoA is 2-fold smaller than that measured in the absence of CoA. We attribute the decrease to the high concentration of CoA (15 mM) that was used in the reaction for the purpose of achieving saturation of the mutant. The simplified kinetic model depicted in Scheme 2 was used in fitting the time course data by curve simulation with KINSIM (25) to show that the k_2 value is significantly reduced (140-fold) whereas the k_1 value is not (Table 4). Thus, the replacement of Asp402 with Ala selectively decreases the efficiency of the second partial reaction. The fact that the 140-fold reduction observed with the D402A is considerably smaller in magnitude than the reduction observed with the D402P mutant (10000-fold) suggests that the flexibility of the Asp402 main chain is more critical to catalysis than is the formation of the Asp402-Arg400 ion pair.

CONCLUSION

The results presented in this paper show that restriction of main chain motion at position 402 greatly impairs the transformation of the 4-CB-AMP intermediate formed in the first partial reaction to the final product 4-CB-CoA formed in the second partial reaction. We interpret this finding as supporting evidence for the proposed role of Asp402 as the hinge that allows the alternation of the C-terminal cap domain between two catalytically active conformations to take place as is required for catalysis of the two-step reaction sequence. Domain alternation in CBL catalysis is necessary because two catalytic residues, Lys492 and His207, that activate the aryl carboxylate for attack on the α-phosphate of ATP in the adenylation reaction must be repositioned to allow the CoA thiol group to attack the benzoyl carbonyl carbon of the 4-CB-AMP intermediate in thioesterification reaction (4, 8). This task is accomplished by rotation of the C-terminal domain, which moves Lys492 greater than 20 Å from the active site and rotates Glu410 into the active site where it acts to pull the side chain of His207 away from the reaction center (*4*, *8*).

SUPPORTING INFORMATION AVAILABLE

A short movie that depicts the steric clash that results from the torsion around the ψ angle of the hinge residue in the absence of the preceding rotation around the ϕ angle. The imine ring of the proline substitution restricts the necessary rotation around ϕ in the D402P mutant protein. This material is available free of charge via the Internet at http://pubs.acs.org.

REFERENCES

1. Chang, K. H., Liang, P. H., Beck, W., Scholten, J. D., and Dunaway-Mariano, D. (1992) Isolation and characterization of the three polypeptide components of 4-chlorobenzoate dehalogenase from Pseudomonas sp. strain CBS-3. *Biochemistry 31*, 5605–5610.
2. Chang, K. H., Xiang, H., and Dunaway-Mariano, D. (1997) Acyl-adenylate motif of the acyl-adenylate/thioester-forming enzyme superfamily: a site-directed mutagenesis study with the Pseudomonas sp. strain CBS3 4-chlorobenzoate:coenzyme A ligase. *Biochemistry 36*, 15650–15659.
3. Dunaway-Mariano, D. and Babbitt, P. C. (1994) On the origins and functions of the enzymes of the 4-chlorobenzoate to 4-hydroxybenzoate converting pathway. *Biodegradation 5*, 259–276.
4. Wu, R., Cao, J., Lu, X., Reger, A. S., Gulick, A. M., and Dunaway-Mariano, D. (2008) Mechanism of 4-chlorobenzoate:coenzyme a ligase catalysis. *Biochemistry 47*, 8026–8039.
5. Gulick, A. M., Lu, X., and Dunaway-Mariano, D. (2004) Crystal structure of 4-chlorobenzoate:CoA ligase/synthetase in the unliganded and aryl substrate-bound states. *Biochemistry 43*, 8670–8679.
6. Conti, E., Stachelhaus, T., Marahiel, M. A., and Brick, P. (1997) Structural basis for the activation of phenylalanine in the non-ribosomal biosynthesis of gramicidin S. *EMBO J 16*, 4174–4183.
7. Gulick, A. M., Starai, V. J., Horswill, A. R., Homick, K. M., and Escalante-Semerena, J. C. (2003) The 1.75 Å crystal structure of acetyl-CoA synthetase bound to adenosine-5′-propylphosphate and coenzyme A. *Biochemistry 42*, 2866–2873.
8. Reger, A. S., Wu, R., Dunaway-Mariano, D., and Gulick, A. M. (2008) Structural characterization of a 140 degrees domain movement in the two-step reaction catalyzed by 4-chlorobenzoate:CoA ligase. *Biochemistry 47*, 8016–8025.
9. Bains, J., and Boulanger, M. J. (2007) Biochemical and structural characterization of the paralogous benzoate CoA ligases from *Burkholderia xenovoran*s LB400: defining the entry point into the novel benzoate oxidation (box) pathway. *J. Mol. Biol. 373*, 965–977.
10. Du, L., He, Y., and Luo, Y. (2008) Crystal structure and enantiomer selection by D-alanyl carrier protein ligase DltA from *Bacillus cereus*. *Biochemistry 47*, 11473–11480.
11. Hisanaga, Y., Ago, H., Nakagawa, N., Hamada, K., Ida, K., Yamamoto, M., Hori, T., Arii, Y., Sugahara, M., Kuramitsu, S., Yokoyama, S., and Miyano, M. (2004) Structural basis of the substrate-specific two-step catalysis of long chain fatty acyl-CoA synthetase dimer. *J. Biol. Chem. 279*, 31717–31726.
12. Jogl, G., and Tong, L. (2004) Crystal structure of yeast acetyl-coenzyme A synthetase in complex with AMP. *Biochemistry 43*, 1425–1431.
13. May, J. J., Kessler, N., Marahiel, M. A., and Stubbs, M. T. (2002) Crystal structure of DhbE, an archetype for aryl acid activating domains of modular nonribosomal peptide synthetases. *Proc. Natl. Acad. Sci. U. S. A. 99*, 12120–12125.
14. Yonus, H., Neumann, P., Zimmermann, S., May, J. J., Marahiel, M. A., and Stubbs, M. T. (2008) Crystal structure of DltA. Implications for the reaction mechanism of non-ribosomal peptide synthetase adenylation domains. *J. Biol. Chem. 283* 32484–32491.

15. Branchini, B. R., Southworth, T. L., Murtiashaw, M. H., Wilkinson, S. R., Khattak, N. F., Rosenberg, J. C., and Zimmer, M. (2005) Mutagenesis evidence that the partial reactions of firefly bioluminescence are catalyzed by different conformations of the luciferase C-terminal domain. *Biochemistry 44*, 1385–1393.
16. Reger, A. S., Carney, J. M., and Gulick, A. M. (2007) Biochemical and crystallographic analysis of substrate binding and conformational changes in acetyl-CoA synthetase. *Biochemistry 46*, 6536–6546.
17. Lovell, S. C., Davis, I. W., Arendall, W. B.3rd, de Bakker, P. I., Word, J. M., Prisant, M. G., Richardson, J. S., and Richardson, D. C. (2003) Structure validation by Cα geometry: φ, ψ and Cβ deviation. *Proteins 50*, 437–450.
18. Gulick, A. M., Horswill, A. R., Thoden, J. B., Escalante-Semerena, J. C., and Rayment, I. (2002) Pentaerythritol propoxylate: a new crystallization agent and cryoprotectant induces crystal growth of 2-methylcitrate dehydratase. *Acta Crystallogr. D Biol. Crystallogr. 58*, 306–309.
19. Leslie, A. G. W. (1992) Recent changes to the MOSFLM package for processing film and image plate data, in *Joint CCP4 + ESF-EAMCB Newsletter on Protein Crystallography, No. 26*.
20. Vagin, A., and Teplyakov, A. (2000) An approach to multi-copy search in molecular replacement. *Acta Crystallogr. D Biol. Crystallogr. 56 Pt 12*, 1622–1624.
21. CCP4. (1994) The CCP4 suite: programs for protein crystallography, *Acta Crystallogr. D Biol. Crystallogr. 50*, 760−763.
22. Murshudov, G. N., Vagin, A. A., and Dodson, E. J. (1997) Refinement of macromolecular structures by the maximum-likelihood method. *Acta Crystallogr. D Biol. Crystallogr. 53* 240–255.
23. Winn, M. D., Isupov, M. N., and Murshudov, G. N. (2001) Use of TLS parameters to model anisotropic displacements in macromolecular refinement. *Acta Crystallogr. D Biol. Crystallogr. 57*, 122–133.
24. Wu, R., Reger, A. S., Cao, J., Gulick, A. M., and Dunaway-Mariano, D. (2007) Rational redesign of the 4-chlorobenzoate binding site of 4-chlorobenzoate: coenzyme a ligase for expanded substrate range. *Biochemistry 46*, 14487–14499.
25. Barshop, B. A., Wrenn, R. F., and Frieden, C. (1983) Analysis of numerical methods for computer simulation of kinetic processes: development of KINSIM–a flexible, portable system. *Anal. Biochem. 130*, 134–145.
26. MacArthur, M. W., and Thornton, J. M. (1991) Influence of proline residues on protein conformation. *J. Mol. Biol. 218*, 397–412.
27. Ho, B. K., Coutsias, E. A., Seok, C., and Dill, K. A. (2005) The flexibility in the proline ring couples to the protein backbone. *Protein Sci. 14*, 1011–1018.
28. Frishman, D., and Argos, P. (1995) Knowledge-based protein secondary structure assignment. *Proteins 23*, 566–579.